Accepted Manuscript

Nanostructured Lipid Carriers as Multifunctional Nanomedicine Platform for Pulmonary Co-Delivery of Anticancer Drugs and siRNA

Oleh Taratula, Andriy Kuzmov, Milin Shah, Olga B. Garbuzenko, Tamara Minko

Nanostructured Lipid Carriers as Multifunctional Nanomedicine Platform for Pulmonary Co-Delivery of Anticancer Drugs and siRNA

Oleh Taratula[1,2], Andriy Kuzmov[1], Milin Shah[1], Olga B. Garbuzenko[1], Tamara Minko[1,3]*

[1]Department of Pharmaceutics, Ernest Mario School of Pharmacy, Piscataway, NJ, 08854

[2]Department of Pharmaceutical Sciences, Oregon State University, Corvallis, OR 97331

[3]The Cancer Institute of New Jersey, New Brunswick, NJ 08903

*Address for Correspondence:

Tamara Minko, Ph.D.

Professor II and Chair
Department of Pharmaceutics
Ernest Mario School of Pharmacy
Rutgers, The State University of New Jersey
160 Frelinghuysen Road
Piscataway, NJ 08854–8020
Phone: 848-445-6348
Fax: 732-445-3134
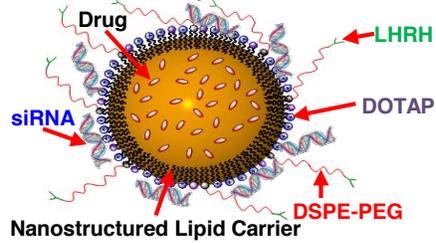Email: minko@rci.rutgers.edu

Abstract

We developed, synthesized, and tested a multifunctional nanostructured lipid nanocarrier-based system (NLCS) for efficient delivery of an anticancer drug and siRNA directly into the lungs by inhalation. The system contains: (1) nanostructured lipid carriers (NLC); (2) anticancer drug (doxorubicin or paclitaxel); (3) siRNA targeted to MRP1 mRNA as a suppressor of pump drug resistance; (4) siRNA targeted to BCL2 mRNA as a suppressor of nonpump cellular resistance and (5) a modified synthetic analog of luteinizing hormone-releasing hormone (LHRH) as a targeting moiety specific to the receptors that are overexpressed in the plasma membrane of lung cancer cells. The NLCS was tested *in vitro* using human lung cancer cells and *in vivo* utilizing mouse orthotopic model of human lung cancer. After inhalation, the proposed NLCS effectively delivered its payload into lung cancer cells leaving healthy lung tissues intact and also significantly decreasing the exposure of healthy organs when compared with intravenous injection. The NLCS showed enhanced antitumor activity when compared with intravenous treatment. The data obtained demonstrated high efficiency of proposed NLCS for tumor-targeted local delivery by inhalation of anticancer drugs and mixture of siRNAs specifically to lung cancer cells and, as a result, efficient suppression of tumor growth and prevention of adverse side effects on healthy organs.

Graphical Abstract

Multifunctional nanostructured lipid carrier-based system (NLCS) for efficient delivery of anticancer drugs, siRNAs and targeting peptide directly into the lung tumor by inhalation.

Drug

LHRH

siRNA

DOTAP

DSPE-PEG

Nanostructured Lipid Carrier

Organ distribution of NLCS

Lungs
Spleen
Kidney
Heart
Liver

1%
9%
8%
23%
59%

Intravenous Injection

4%
0%
0%
13%
83%
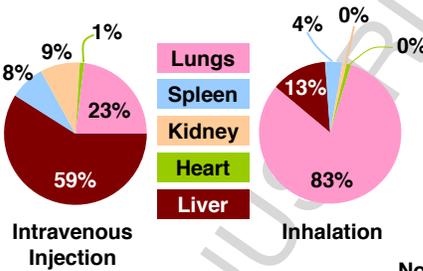
Inhalation

Distribution of non-targeted and targeted NLCS in tumor and healthy lung tissues after inhalation

Tumor Tissue

Light

Non-Tumor Tissue

Fluorescence

Non-targeted NLCS

LHRH-NLCS

3
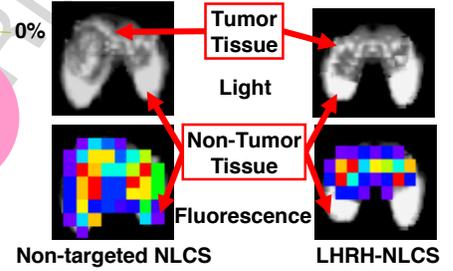
Introduction

Lung cancer is the leading cancer killer in both men and women. Despite advantages in surgical lung cancer treatment, chemotherapy continues to play an important role as primary and supportive care in treating lung cancer [1-5]. Conventional intravenous chemotherapy usually employs high doses of toxic drugs which often induce severe adverse side effects on healthy organs. Alternatively, oral delivery of anticancer drugs for lung cancer treatment is usually compromised by poor bioavailability of the drug for lung cancer cells and its degradation during the first-pass metabolism. Therefore, an ideal therapy of lung cancer would provide for the administration of high doses of drugs specifically to the lung tumor tissues via the inhalation for the maximum treatment efficiency and low adverse side effects. The most important advantages of the pulmonary route for drug administration are a large absorptive surface of lungs for aerosol deposition, avoidance of the first-pass metabolic degradation, limited penetration of inhaled drug(s) into the systemic circulation and, as a result, fewer adverse side effects on healthy organs. Several formulations of traditional anticancer drugs were already adopted for the local inhalation delivery [6-9]. However, despite the advantages, the efficient inhalation delivery currently is possible for only a limited number of drugs. In addition, the efficacy of chemotherapy is also limited by the rapid development of tumor resistance. The mechanisms of this resistance are common to most cancers and include "pump" and "nonpump" drug resistance [10, 11]. The pump resistance is caused by membrane transporters that pump out drugs from cells, decreasing the efficacy of the treatment [12-16]. The main mechanism of nonpump resistance is an activation of cellular antiapoptotic defense [10, 11, 17-20]. Recently, we showed that siRNA can be effectively used for the suppression of proteins, responsible for both pump and nonpump drug resistance in different cancer cells including lung cancer cells [17, 20-22]. Consequently, the development of nanomedicine platform capable of tumor targeted combinatorial delivery of anticancer drugs and siRNA as suppressors of pump and nonpump cellular resistance via pulmonary route is highly desirable. Recently, several different nanocarriers have been developed for inhalation delivery of different drugs and nucleic acids [22-24]. However, used carriers, especially liposomes, have some drawbacks, in particular for the efficient delivery of siRNA. In order to circumvent these salient weak points, we designed Nanostructured Lipid Carriers (NLC) for inhalation delivery of anticancer drugs
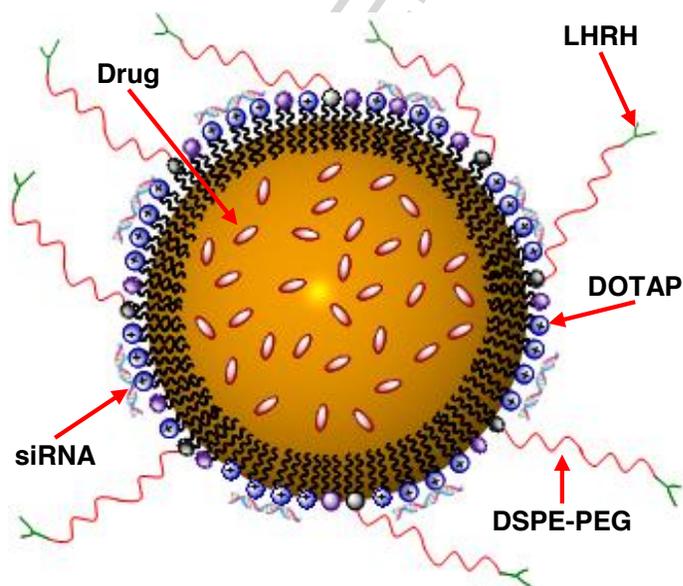

Figure 1. A schematic representation of Nanostructured Lipid Carrier (NLC)-based drug delivery system for pulmonary co-delivery of an anticancer drug, siRNA and targeting peptide.

4

and siRNA. NLC are a new generation of lipid nanoparticles, which are developed through the combination of advantages from different nanocarriers including liposomes [25]. The proposed NLC based system (NLCS) was designed to fulfill the following tasks: (1) to provide local inhalation lung delivery of active components; (2) to suppress pump and nonpump resistance; (3) to offer targeted drug delivery specifically to the cancer cells and (4) to limit adverse side effects on healthy lung tissues and other organs. Consequently, we designed a highly efficient NLCS for inhalation therapy which contains five main components: (1) NLC as the carriers; (2) anticancer drug; (3) siRNA targeted to MRP1 mRNA as a suppressor of pump drug resistance; (4) siRNA targeted to BCL2 mRNA as a suppressor of nonpump cellular resistance and (5) a modified synthetic analog of luteinizing hormone-releasing hormone (LHRH) as a targeting moiety specific to the receptors that are overexpressed in the plasma membrane of lung cancer cells (Fig 1).

Materials and methods

Materials

Precirol ATO 5 was generously provided by Gattefossé USA (Paramus, NJ). Soybean phosphatidylcholine (SPC), Doxorubicin (DOX), Paclitaxel (TAX), Triethylamine (TEA), Squalene, Tween-80, Mannitol were purchased from Sigma Aldrich (St. Louis, MO). DSPE-PEG-NH$_2$ (1,2-distearoyl-*sn*-glycero-3-phosphoethanolamine-N-[amino(polyethylene glycol)-2000] (ammonium salt)), DSPE-PEG-COOH (1,2-distearoyl-*sn*-glycero-3-phosphoethanolamine-N-[carboxy(polyethylene glycol)-2000] (ammonium salt)) and DOTAP (1,2-dioleoyl-3-trimethylammonium-propane (chloride salt)) were obtained from Avanti Polar Lipids (Alabaster, AL). Cy5.5 NHS ester was purchased from GH Healthcare Life Sciences (Piscataway, NJ). A modified synthetic analog of Luteinizing Hormone-Releasing Hormone (LHRH) decapeptide (Gln-His-Trp-Ser-Tyr-DLys(D-Cys)-Leu-Arg-Pro) was synthesized according to our design by American Peptide Company, Inc. (Sunnyvale, CA). The sequence of native LHRH peptide, which is similar in human, mouse, and rat, was modified to provide a reactive amino group only on the side chain of a lysine residue, which replaced Gly at the position 6 to yield the superactive, degradation-resistant-Lys-6-des-Gly-10-Pro-9-ethylamide LHRH analog [19, 26]. The synthesized sequence of LHRH peptide is highly efficient for targeting of drug delivery systems specifically to the cancer tumors [18-20, 27, 28] and Cys residue do not influence the recognition process. The sequences of siRNA targeted to BCL2 (sense strand: 5′-GUG-AAG-UCA-ACA-UGC-CUG-CdTdT-3′; antisense strand: 5′-GCA-GGC-AUG-UUG-ACU-UCA-CdTdT-3') and MRP1 (sense strand: 5′-GGC-UAC-AUU-CAG-AUG-ACA-CdTdT-3′; antisense strand: 5′-GUG-UCA-UCU-GAA-UGU-AGC-CdTdT-3') mRNA were custom synthesized according to our design by Ambion (Austin, TX).

Cell line

A549 human lung adenocarcinoma cells were obtained from the ATTC (Manassas, VA); A549 cells transfected with luciferase were purchased from Xenogen Bioscience, (Cranbury, NJ). Cells were cultured in RPMI 1640 medium (Sigma, St. Louis, MO) supplemented with 20% fetal bovine serum (Fisher Chemicals, Fairlawn, NJ) and 1.2 mL/100 mL penicillin–streptomycin (Sigma, St. Louis, MO). Cells were grown at 37 °C in a humidified atmosphere of 5% CO_2 (v/v) in air. All experiments were performed on cells in the exponential growth phase.

5

Preparation of NLC

Drug loaded NLC were prepared by a modified melted ultrasonic dispersion method [29, 30]. Prior to the NLC preparation, the doxorubicin hydrochlorate (DOX·HCl) was stirred with twice the molar amount of TEA in DMSO for 12 h to obtain lipophilic DOX base [31]. Typically, DOX base or TAX dissolved in 1 mL of DMSO was added to the hot lipid phase consisted of 100 mg Precirol ATO 5 (solid lipid), 100 mg Squalene (liquid lipid) and 5 mg SPC (lipophilic emulsifier). Aqueous phase was prepared by dissolving 250 mg Tween-80 (surfactant) and 25 mg DOTAP (cationic lipid) in 10 mL of DI water. In order to prepare PEG coated NLC, 10 mg DSPE-PEG-COOH was additionally added to the aqueous phase. Both phases were maintained for 15 min at 80 °C in the oil bath under magnetic stirring. Then the hot lipid phase was added slowly to the aqueous solution and dispersed using a high-speed homogenizer (PRO Scientific Inc. Oxford, CT) for 5 min at 12,000 RPM. The crude emulsion was additionally treated by a probe type ultrasonicator (Fisher Scientific Model 120 Sonic Dismembrator) for 5 min at 3 W. Then, the hot emulsion was cooled at 4 °C on an ice bath, maintaining the mechanical stirring for 60 min. After preparation, the NLC were purified by dialysis (MWC 10,000) and subjected to lyophilization. Mannitol (5%) was added into NLC suspension as cryoprotector. The obtained powder was stored at 4 °C until further use.

Preparation of fluorescence labeled and LHRH targeted NLC

Prior preparation of targeted NLC, DSPE-PEG-NH$_2$ and DSPE-PEG-COOH were conjugated with Cy5.5 and LHRH peptide, respectively, as previously described [27, 32]. LHRH targeted NLC (a), Cy5.5 labeled NLC (b) or Cy5.5 labeled and LHRH targeted NLC (c) were prepared by adding (a) 10 mg of DSPE-PEG-LHRH, (b) 10 mg of DSPE-PEG-COOH : DSPE-PEG-Cy5.5 (10:1) and (c) 10 mg of DSPE-PEG-LHRH : DSPE-PEG-Cy5.5 (10:1) to the hot lipid phase instead of DSPE-PEG-COOH, respectively.

Preparation of siRNA-NLC complexes

The siRNA complexes were prepared at w/w (weight NLC/weight siRNA) ratio of 117:1 in water by adding stock solution of NLC into a prepared siRNA solution (BCL2 siRNA: MRP1 siRNA = 1:1). The weight ratio (siRNA/NLC) was determined from Ethidium Bromide (EtBr) dye displacement assay. The final concentrations of siRNAs (BCL2:MRP1 =1:1) and drug loaded NLC in the solution were 128.5 μg/mL and 15 mg/mL, respectively. The samples were vortexed, and the solutions were then incubated at room temperature for 30 min to ensure complex formation. It should be stressed that lipid composition of both siRNA loaded and siRNA free NLC was the same in our study.

Particle size, shape, zeta potential and cytotoxicity

The particle size distribution and the zeta potential of the prepared NLC were measured by Malvern ZetaSizer NanoSeries (Malvern Instruments, UK) according to manufacturer instructions. All measurements were carried out at room temperature. Each parameter was measured five times, and average values and standard deviations were calculated. The shape of the NLC was determined by Atomic Force Microscope (AFM) as previously described [33]. In order to image the prepared NLC, 5 μL of the solutions were deposited on freshly cleaved mica. After 5 minutes of incubation, the mica surface was rinsed with 3 drops of DI water for 4 times and dried under a flow of dry nitrogen. The samples of the

condensates were imaged with a tapping mode atomic force microscope (Nanoscope III A, Digital Instruments, Santa Barbara, CA). Cytotoxicity of nanoperticles was analyzed using a modified 3-(4, 5-dimethylthiazol-2-yl)-2, 5-diphenyltetrazolium bromide) (MTT) assay as previously described [10, 11, 17].

Evaluation of NLC condensation ability by ethidium bromide dye displacement assay

Fluorescence titration of siRNA/EtBr with the complexation agents were performed as previously described [21]. The complexes were prepared by the intercalation of siRNA with EtBr at 4:1 ratio (siRNA base pairs to EtBr) in water. 1 µL aliquots of 20 mg/mL NLC were sequentially added to 0.4 µM solution of siRNA in 180 µL water containing EtBr. After each addition, the mixture was stirred and the fluorescence of the solution was measured (590 nm emission; 490 nm excitation). Binding NLC caused a displacement of bound EtBr, resulting in a decrease in the fluorescence emission intensity.

Determination of siRNA binding to NLC by agarose gel retardation assay

siRNA binding to LHRH-Drug-NLC was evaluated by agarose gel retardation assay as previously described [21]. siRNA-NLC complexes were prepared at different w/w ratios: 1:10, 1:50, 1:100, 1:117. The samples were further diluted with water, electrophoresed in 4 % agarose gel at 100 mV for 60 min in DPBS and stained with EtBr. The gels were digitally photographed and scanned using the Gel Documentation System 920 (Nucleo-Tech, San Mateo, CA).

Orthotopic lung cancer model, imaging and treatment

All animal experiments were carried out according to the approved protocol and institutional guidance. A mouse orthotopic model of human lung cancer previously developed in our laboratory [22, 23, 34] was used in the current study. Briefly, athymic nu/nu mice (NCRNU-M, CrTac:NCr-Foxn1nu) were purchase from Taconic Farms, Inc (Cranbury, NJ). A549 human lung adenocarcinoma epithelial cells (5-8 $\times$ 10^6) transfected with luciferase were re-suspended in 0.1 mL of RPMI medium containing 20% fetal bovine serum, mixed with 5 µl of EDTA and were administered to the mouse lungs through a catheter. The development of tumor growth was monitored and tumor volume was calculated by different imaging systems in live animals. All imaging procedures were performed under inhalation anesthesia with isoflurane at a concentration of 4% for induction of anesthesia and 1–2% for maintenance. Mice were placed in prone position with isoflurane supplied via a nose cone. After image data acquisition, the recovery time of the animals from anesthesia was usually less than five minutes. Optical imaging was performed using *In-Vivo* bioluminescent IVIS (Xenogen, Alameda, CA) and MS FX PRO® (Carestream Molecular Imaging, Woodbridge, CT) systems. In order to visualize cancer cells transfected with luciferase, luciferin was injected intraperitoneally in dose of 150 mg luciferin/kg of body weight 10 -15 minutes before imaging. The quantitative analysis of tumor size and volume using optical imaging system was described previously [34]. Magnetic Resonance Imaging (MRI) was performed using a 1 T M2™ whole body scanner (Aspect Imaging, Shoham, Israel). T2 weighted images (repetition time 2607 ms, echo time 44 ms) were recorded in Fast Spin Echo sequence. At a spatial resolution of 312 micron, the tumors were coronal imaged in a single section through the lung using an image matrix of 256 × 256, a field of view of 80 mm^2, and 4 excitation. Tumor volume was calculated using Vivoquant 1.21 software. The Computed Tomography (CT) scan was done with Albira high-resolution PET/computed

7

tomography scanner (Carestream Molecular Imaging, Woodbridge, CT). The scan parameters were set as follow: tube voltage 45 kVp, tube current 400 µA, FOV 70 x 70 mm, detector pixels 2400 x 2400. Total scan duration was about 12 minutes. Image data was reconstructed using the FBP algorithm. The resulting voxel size of the isotropic dataset was 125 microns. CT datasets were visualized using the software packages PMOD 3.3 (PMOD Technologies) and Volview 3 (Kitware Inc., Clifton Park, NY). Ultrasound imaging was carried out using Vevo 2100 system (VisualSonics, Toronto, Canada). Tumor size and volume was calculated in 2- and 3-dimensional images using manufacture software. Four-six weeks after the instillation of tumor cells, when the tumor in lungs reached a volume of about 40 mm^3, mice were treated on days 0, 3, 7, 11, 14, 17, 21, and 24 using previously developed regimen and nose-only exposure chamber for inhalation of small laboratory animals [34, 35]. The following series of experiments were carried out: (1) Untreated mice (control); (2) mice treated by intravenous injection of TAX; mice treated by inhalation with: (3) LHRH-NLC; (4) LHRH-NLC-TAX; (5) LHRH-NLC-TAX-siRNAs (targeted to MRP1 and BCL2 mRNAs). The dose of TAX in all drug-containing formulations was 2.5 mg/kg for the single administration. This dose corresponds to the maximum tolerated dose (MTD) of LHRH-SLN-TAX delivered by inhalation. The MTD was estimated in separate experiments based on animal weight change after the instillation of increasing doses of drug formulation as previously described [19, 34, 36]. The dose of siRNA was 170 µg/kg for the single administration. The dose of free non-bound TAX used for intravenous injection was also 2.5 mg/kg. Animal weight was monitored every day during the treatment period. After the treatment, all mice were anesthetized with isoflurane and euthanized. The organs (lungs, heart, liver, kidney, spleen, and brain) were excised and used for further analysis. Changes in tumor volume were used as an overall marker for antitumor activity.

Distribution of NLC in different organs, normal and tumorous lung tissues

Organ distribution labeled by Cy5.5 NLC was studied as previously described [22, 23, 27, 34]. Briefly, animals were anesthetized with isoflurane using the XGI-8 Gas Anesthesia System (Xenogen, Alameda, CA). Fluorescence of labeled with Cy5.5 NLC was visualized 24 h after the i.v. injection or by inhalation using IVIS imaging system. Visible light and fluorescence images were taken and overlaid using the manufacturer's software to obtain composite images. The distribution of fluorescence in different organs (liver, kidney spleen, heart, brain and lungs) was analyzed using original software developed in our laboratory. After sacrificing animals, lungs were excised, washed in ice-cold saline and kept frozen. LHRH-targeted Cy5.5-TAX-NLC-siRNA accumulation in lung tissues (tumorous and healthy) was visualized by fluorescence microscopy (Olympus America Inc., Melville, NY) on frozen 5 mm tissue sections as described [36].

Accumulation of NLC in lung tumor, cellular uptake and localization of drug and siRNA

Internalization of osmium-labeled NLC by lung cells was studied by electron transmission microscopy in lung tissue sections fixed prior to microscopy using standard techniques as previously described [16, 37, 38]. Briefly, lung tissue slices were fixed for 2 h in Trump's EM Fixative (combination of low concentration of both formaldehyde and glutaraldehyde in 0.1 M Milloning's Phosphate buffer pH 7.3). Postfixation was carried out in 1% Osmium Tetroxide in buffer for 1 h followed by dehydration in graded Ethanol series and embedded in Spurr's Low Viscosity Resin. Sections were prepared using a diamond knife by LKB-

8

2088 Ultramicrotome (LKB-Produkter / Bromma, Sweden). Observation and micrographs were made with a JEM-100CXII Electron Microscope. (Jeol Ltd., Tokyo, Japan). Fluorescent dye-labeled siRNA was synthesized by Ambion according to our design through the conjugation of FAM dye (green color) to the 5' siRNA antisense strand. Intrinsic fluorescent of DOX (red color) was employed for the detection of drug internalization into the cancer cells. Prior to the visualization, A549 cells were plated (10 000 cells/well) in 6-well tissue culture plate and incubated with the studied formulation for 3 h. In addition, cell nuclei were stained by a nuclear dye (4', 6-diamidino-2-phenylindole, DAPI, Sigma Chemical Co., St. Louis, MO). Cellular internalization of LHRH-DOX-NLC-siRNA complexes were analyzed by a fluorescence microscope (Olympus America Inc., Melville, NY) as previously described [21, 39].

Suppression of targeted mRNA

The expression of BCL2 and MRP1 mRNA was analyzed by quantitative reverse transcription-polymerase chain reaction (RT-PCR). The following pair of primers were used: *BCL2* − GGA TTG TGG CCT TCT TTG AG (sense), CCA AAC TGA GCA GAG TCT TC (antisense); *MRP1*− ATG TCA CGT GGA ATA CCA GC (sense), GAA GAC TGA ACT CCC TTC CT (antisense); *β2-m* (internal standard)− ACC CCC ACT GAA AAA GAT GA (sense), ATC TTC AAA CCT CCA TGA TG (antisense). The extraction of RMA and RT-PCR were performed as previously described [11, 22].

Statistical analysis.

Data were analyzed using descriptive statistics, single-factor analysis of variance (ANOVA), and presented as mean values ± standard deviation (SD) from four to eight independent measurements. The comparison among groups was performed by the independent sample student's *t*-test. The difference between variants was considered significant if $P < 0.05$.

Results

Preparation of drug loaded, tumor targeted NLC

In the current study, drug-loaded, cationic NLC were successfully prepared using DOX or TAX as the model chemotherapeutic agents. Due to intrinsic fluorescence of DOX, it was primarily selected to evaluate uptake and intracellular localization of anticancer drugs delivered by NLCS. On the other hand, TAX was used to assess anticancer efficacy of the developed NLCS. To facilitate the entrapment efficiency of positively charged DOX in the oil phase, DOX
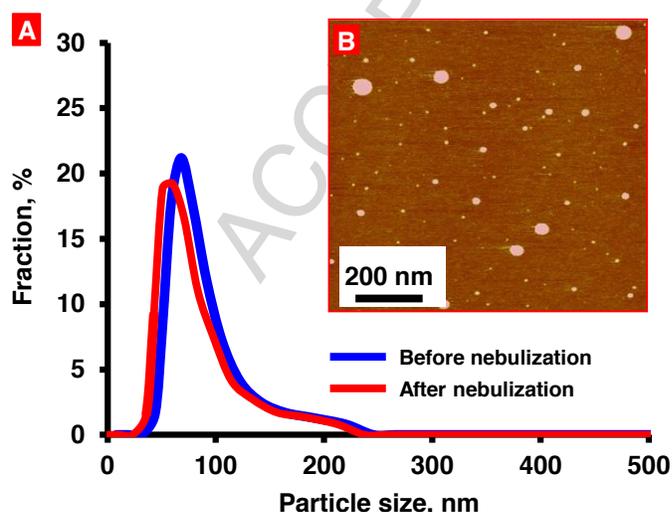
Figure 2. Characterization of LHRH-targeted paclitaxel (TAX)-loaded Nanostructured Lipid Carriers (LHRH-NLC-TAX-siRNA). (A) Size distribution of LHRH-NLC-TAX-siRNA measured by dynamic light scattering before and after nebulization. (B) Atomic Force Microscope image of LHRH-NLC-TAX-siRNA.

base was prepared by mixing DOX hydrochloride with negatively charged TEA as previously reported [31]. Using the centrifugation ultrafiltration method, it was demonstrated that drug loading of nanoparticles was 5 w/w% for both DOX base and TAX (5 µg of drug per 100 µg of lipid). Dynamic light scattering and atomic force microscopy studies revealed that the drug loaded NLC were 110 ± 20 nm in diameter with polydispersity index of 0.4 (Fig. 2A). The most optimal regimen of nebulization was previously selected in our laboratory in order to avoid nanoparticle destruction and release of drug and siRNA [40]. The measurement of particle size distribution before and after nebulization showed that nebulization did not influence the stability of the nanoparticles and conjugated siRNA (Fig. 2). As AFM measurements demonstrated (Fig.2B), spherical nanoparticles were the predominant products, as seen on mica surfaces. (Fig. 2A and B). A 30-day physical stability test of the drug-NLC at 4 °C was also conducted and no statistical difference was found in the particle size over time. In order to enhance steric stability of NLCS and reduce its uptake by cells of reticuloendothelial system, the NLC surface was modified with PEG. Furthermore, a synthetic analog of LHRH peptide was conjugated to the distal end of DSPEG-PEG-COOH via amide bond formation as a ligand to corresponding LHRH receptors that are overexpressed in the plasma membrane of many types of cancer cells [18, 19, 27, 28, 39, 41] to direct the NLCS specifically to the lung cancer cells and limit the adverse cytotoxic side effects of chemotherapy on healthy organs and non-cancerous lung tissues.

Characterization of siRNA complexation efficiency of NLC
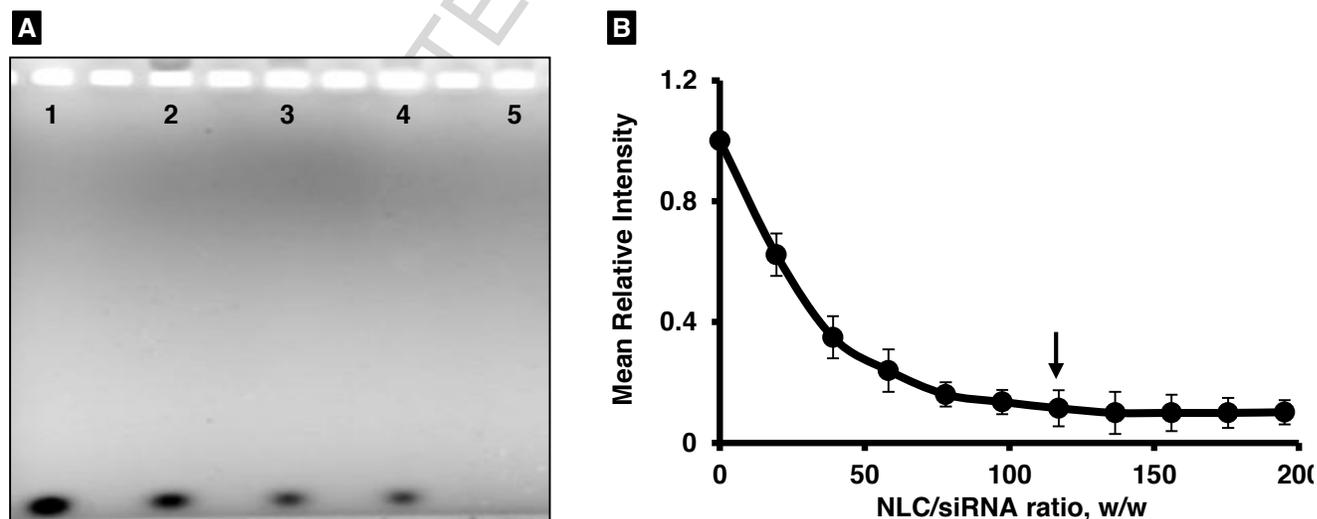

Figure 3. Complexation of siRNA with NLC. (A) A representative agarose gel electrophoresis image illustrating siRNA complexation efficiency by LHRH-NLC-TAX at the following w/w ratio (weight NLC/weight siRNA): (1) 0:1 (naked siRNA, control); (2) 10:1; (3) 50:1; (4) 100:1; and (5) 117:1. Complexation of siRNA prevented staining of siRNA by ethidium bromide and led to the disappearance of the siRNA band. Therefore, the fluorescent intensity of the siRNA band on the gel (well 5) disappeared when siRNA was complexed with NLC at w/w ratio = 117:1. (B) siRNA complexation efficiency of LHRH-NLC-TAX evaluated by the ethidium bromide dye displacement assay. The arrow on the curve highlights the w/w ratio corresponding to the apparent end of siRNA complexation with NLC. Means ± SD are shown.

10

The developed NLCS was aimed to suppress multidrug resistance in cancer cells by siRNA targeted to proteins responsible for cellular resistance. In most lung cancers, this resistance is usually associated with the overexpression of (1) MRP1 protein responsible for drug efflux from the cancer cells (pump resistance) and (2) BCL2 protein that is responsible for antiapoptotic cellular defense (non-pump resistance) [11, 17, 22, 34]. Consequently, we incorporated two types of siRNA targeted to MRP1 and BCL2 mRNA into the proposed NLCS for the effective suppression of cellular resistance. To this end, we made NLC positively charged via the incorporation of DOTAP as cationic lipid into the nanoparticle structure. Since, efficiency of siRNA condensation depends only on the amount of polycations and does not rely on siRNA sequence; the developed NLC could be used for simultaneous condensation of siRNA molecules targeted to both MRP1 and BCL2 genes. The efficiency of the prepared NLC to bind and form complexes with siRNA molecules via electrostatic interaction was determined by agarose gel retardation and ethidium bromide dye displacement assays (Fig. 3). We found that the complete condensation of siRNA was achieved at the ratio of NLC to siRNA (weight/weight) around 117:1 leading to the disappearance of siRNA band on the agarose gel (Fig. 3A) and decrease in the fluorescence of ethidium bromide down to the background level (Fig. 3B). Consequently, this NLC/siRNA ratio was used to form NLC-siRNA complexes that were further used in the following investigations.

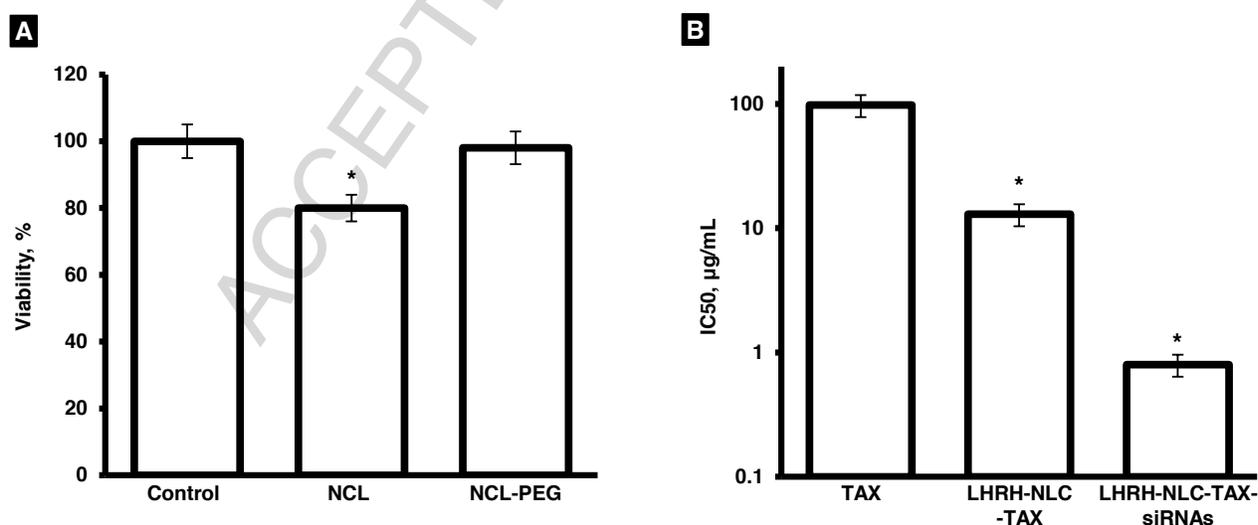### *Zeta potential and cytotoxicity*

Figure 4. Viability of multidrug-resistant H69AR human lung cancer cells incubated for 48 hours with the indicated formulations. A, cytotoxicity of formulations that do not contain DTAX; B, cytotoxicity of formulations that contain TAX. Means ± SD are shown. *$P < 0.05$ when compared with control.

The measurement of cellular viability showed that positively charged NLC (+ 60.3 mV) demonstrated a signs of cytotoxicity (Fig. 4A, bar 2). The viability of cells incubated with NLC decreased by approximately 20% ($P < 0.05$ when compared with control). Caging of
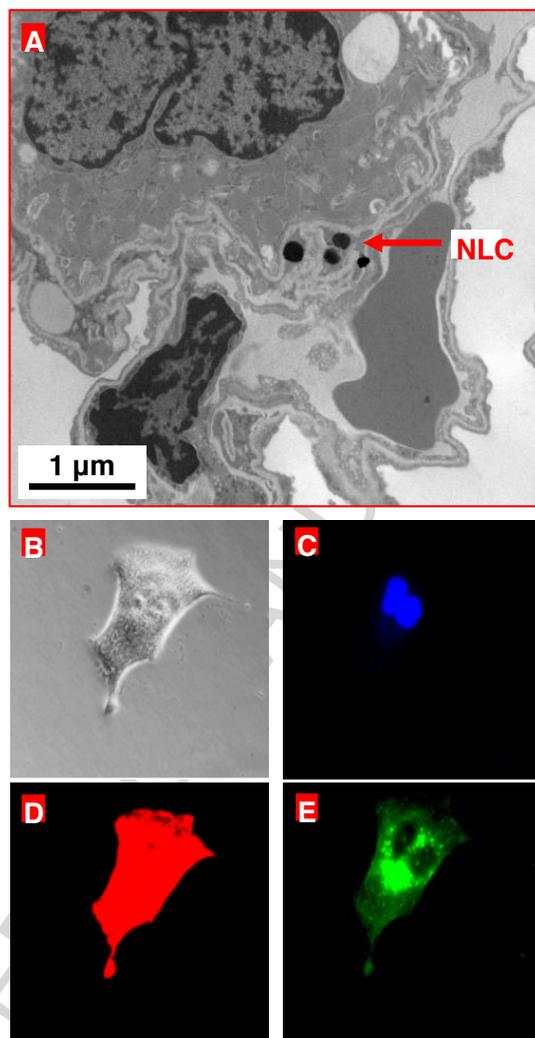
Figure 5. Accumulation of LHRH-NLC in the lung tissues after the inhalation delivery (A) and intracellular localization of the drug and siRNA released from NLC (B-E). Representative transmission electron microscopy image of LHRH-targeted NLC labeled with osmium tetroxide in lung tissues (A). Representative images of A549 human lung cancer cells incubated 3 h with LHRH-NLC-DOX-siRNA: (B) visible light; (C) fluorescence images of nuclei stained with DAPI; (D) and (E) cellular localization of DOX (red fluorescence) and fluorescently labeled siRNA (green fluorescence), respectively.

nanoparticles with PEG eliminated this effect (Fig. 4A, bar 3). Zeta potential of NLC-siRNA complexes decreased to +45.5 mV while caging with PEG almost completely eliminated the charge of nanoparticles. In contrast, nanoparticles containing the drug were highly toxic. The data obtained show that incorporation of TAX into tumor-targeted nanoparticles increased its toxicity to cancer cells overexpressed LHRH receptors in 7.5 times (Fig. 4B, compare bars 2 and 1). Simultaneous suppression of BCL2 and MRP1 proteins by siRNA led to the further enhancement in cytotoxicity of an entire complex. In fact, cytotoxicity of LHRH-NLC-TAX-siRNAs (MRP1 and BCL2) complexes was 120 and 16 times higher when compared with free drug and LHRH-NLC-TAX, respectively (Fig. 4B, bar 3).

12

Intracellular delivery of anticancer drug and siRNA

In order to study the penetration of NLC in lung tissues after inhalation, lipids were labeled by osmium tetroxide and visualized in slices of lung tissues by transmission electron microscopy (Fig. 5A). These data clearly showed that NLC did penetrated lung cells after inhalation and accumulated in the cytoplasm. To evaluate the penetration of NLCS into cancer cells and the intracellular localization of delivered siRNA and DOX (intrinsic red fluorescence), LHRH-DOX-NLC was complexed with FAM-labeled siRNA (green fluorescence) and then incubated with A549 human lung cancer cells for 3 h. This study demonstrated that the developed NLCS successfully delivered chemotherapeutic drug and siRNA into human A549 lung cancer cells (Fig. 5B-E). The analysis of intracellular localization by fluorescence microscopy showed that siRNA was predominantly localized in the cytoplasm (Fig. 5E), while DOX was evenly distributed in all cellular compartments: cytoplasm and nuclei (Fig. 5D).

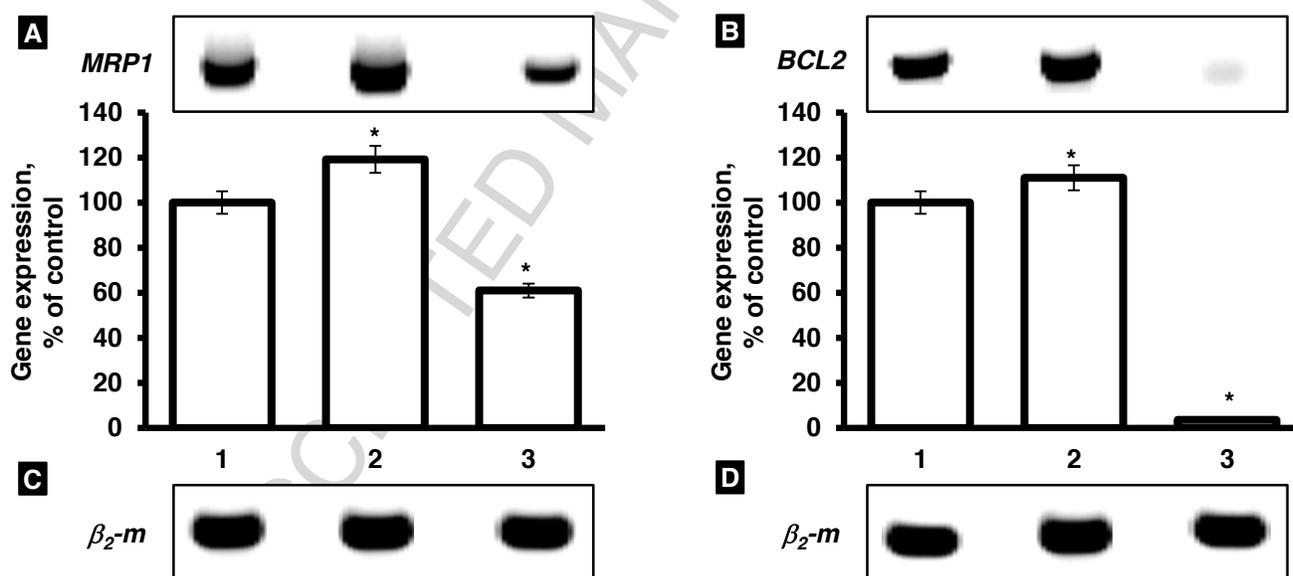### Suppression of targeted genes by siRNA

Figure 6. Expression of *MRP1* (A), *BCL2* (B) and β_2-*m* (C and D, internal standard) genes. Representative images of RT-PCR products and densitometric analysis of bands in A549 lung cancer cells incubated with the following formulations: (1) Control (medium); (2) LHRH-NLC-TAX; and (3) LHRH-NLC-TAX-siRNAs (MRP1 and BCL2). Gene expression in control was set to 100%. Means ± SD are shown. *$P < 0.05$ when compared with control.

The ability of siRNA molecules delivered by NLC to silence the targeted mRNA was investigated using RT-PCR. In these experiments, the expression of targeted *BCL2* and *MRP1* genes was evaluated in mRNA isolated from A549 human lung cancer cells incubated with LHRH-TAX-NLC and LHRH-TAX-NLC-siRNA (BCL2 and MRP1) for 24 h. Data obtained showed that treatment of lung cancer cells with LHRH-TAX-NLC significantly ($P < 0.05$) increased the expression of both MRP1 and BCL2 mRNA responsible for pump and nonpump cellular drug resistances, respectively (Fig. 6A and B, band and bar 2). Remarkably, siRNA molecules concurrently delivered with TAX by NLC targeted to cancer cells by LHRH led to the significant ($P < 0.05$) decrease in the expression of the *BCL2* and

MRP1 genes when compared with control cells and cells incubated with free TAX (Fig. 6A and B, band and bar 3). Consequently, siRNA delivered by the proposed NLC preserved its ability to suppress targeted mRNA.

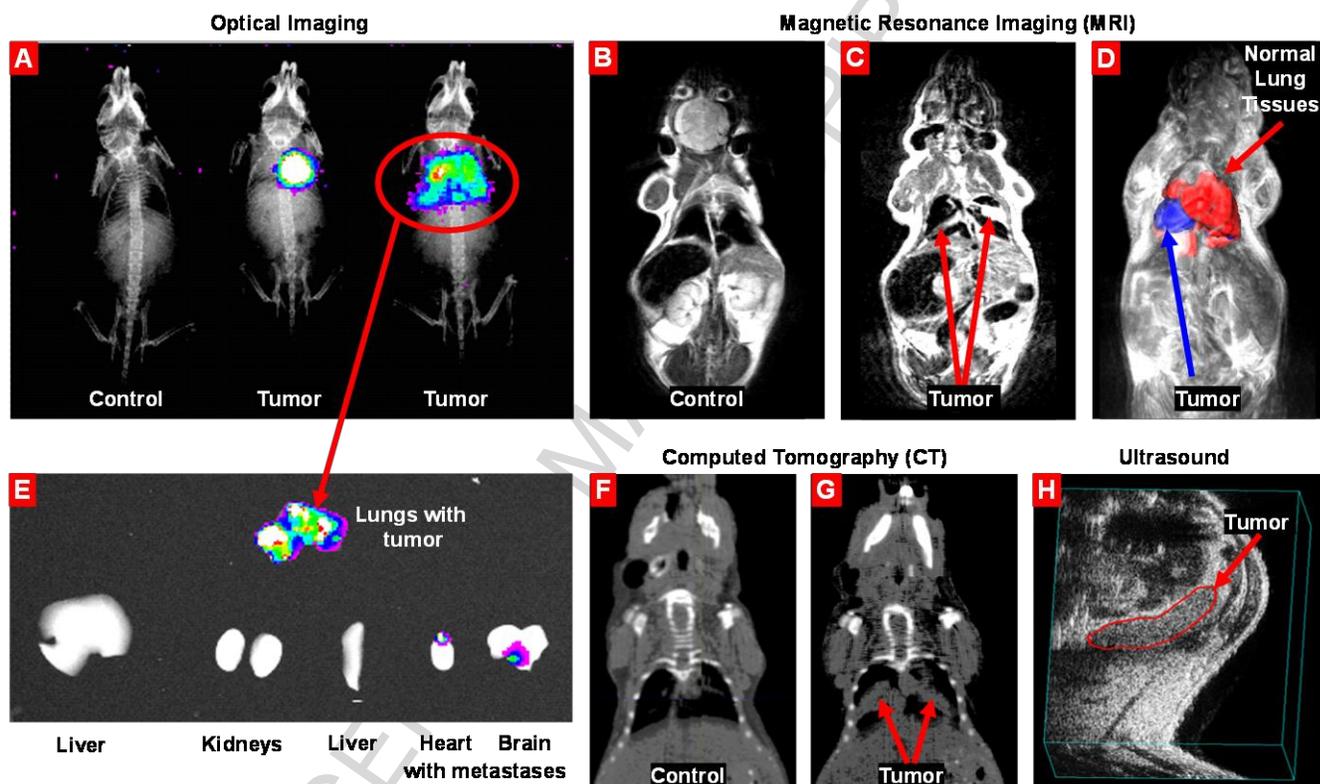***Validation of orthotopic model of lung cancer***

Figure 7. Evaluation of orthotopic lung cancer model by imaging. (A) Bioluminescence optical imaging of control mouse and mice with lung tumors of different size. (B-D) Magnetic resonance imaging of control mouse (B) and mice with lung tumors of different size (C, D). Lung tumor (blue) and healthy lung tissues (red) are shown (D). (E) Optical imaging of excised organs. (F-G) Computed tomography images of control mouse (F) and mouse with lung tumors (G). (H) Visualization of lung tumor by ultrasound imaging system.

The development of orthotopic mouse model of human lung cancer was confirmed by several independent imaging techniques including optical imaging of lung cancer cells transfected with luciferase and tumors, MRI, CT and ultrasound imaging systems. Optical imaging (Fig. 7A) clearly confirmed the growth of lung cancer in one or, most often, both lungs. In addition to imaging of entire animal, lungs, liver, kidneys, heart and brain were excised and imaged by the same optical imaging system (Fig. 7E). Images of these organs show growth of tumor cells in the lungs. Moreover, approximately in 5% of animals, cancer cells were detected in the heart and brain demonstrating the development of metastases. MRI (Fig. 7B-D), CT (Fig. 7F-G) and ultrasound (Fig. 7H) images confirmed the development of lung tumor.

Body distribution and accumulation of NLC in the lungs

A Collision nebulizer connected to four-port, nose-only exposure chambers was used for inhalation delivery of the developed NLCS labeled Cy5.5 into nude mice with lung cancer. Organ distribution of non-targeted NLCS was studied using the IVIS imaging system 24 h after a single inhalation or i.v. administration (Fig.8). It was found that inhalation delivery substantially enhanced lung exposure to non-targeted NLCS and limited the accumulation of the same system in other organs when compared with i.v. administration (Fig. 8A). Thus, the total amount of non-targeted NLC-TAX-siRNA retained in the lungs after inhalation (83%) was more than 3.5 times higher when compared with *i.v.* injection of the same nanoparticles (23%) (Fig. 8A). Targeting of nanoparticles by LHRH peptide does not influence significantly on the distribution of nanoparticles within organs without tumor. However, more detailed analysis showed that in contrast to non-targeted NLCS that was distributed uniformly through the lungs after the inhalation, inhaled LHRH-targeted NLCS predominately accumulated in the lung tumor avoiding healthy lung tissues (Fig. 8B). The data obtained by the IVIS imaging system were confirmed by the fluorescence microscope analysis of labeled (red fluorescence) NLC (Fig. 8C). These data demonstrated that NLC targeted specifically to cancer cells accumulated predominately in the areas of lungs contained tumor cells, keeping non-tumorous lung tissues intact.
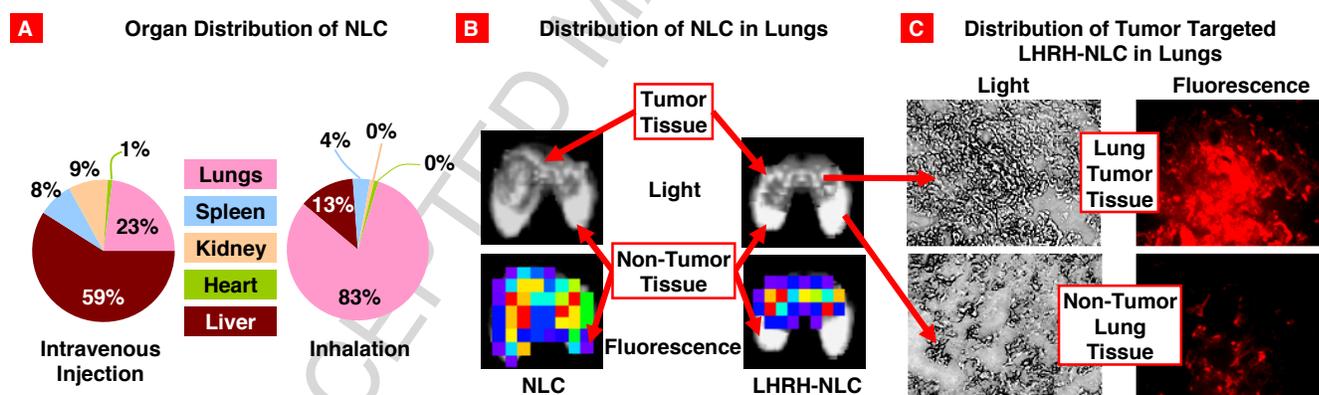

Figure 8. Accumulation of NLC in the lungs and other organs. (A) Organ distribution of fluorescently labeled (Cy5.5) NLC in mice after *i.v.* (left) and inhalation (right) administration. (B) Distribution of fluorescently labeled (Cy5.5) non-targeted and LHRH-tumor targeted NLC in mouse lungs bearing human lung cancer. (C) Distribution of fluorescently labeled (Cy5.5) LHRH-tumor - targeted (NLC-LHRH) in mouse lungs bearing human lung tumor cells (tumor and non-tumor tissues; bright field and fluorescence microscope images; red color represents distribution of NLC-LHRH in tumor and non-tumor lung tissues).

Antitumor activity

The results of the measurement of tumor volume using imaging during the treatment of lung cancer with developed NLCS and corresponding controls are presented in Fig. 9. It was found that in untreated animals, lung tumor progressively grew reaching 117.1 ± 18.7 mm^3 (curve 1 in Fig.9) at the end of the experiments (day 24 after the beginning of the treatment in other experimental groups). Inhalation treatment (8 times within 4 weeks) of mice with lung cancer by LHRH-NLC alone that did not contain an anticancer drug (curve 2 in Fig. 9) did not change significantly the progression of lung tumor leading to the increase of its volume up to 113.6 ± 1.5 mm^3 ($P > 0.05$ when compared with untreated control).
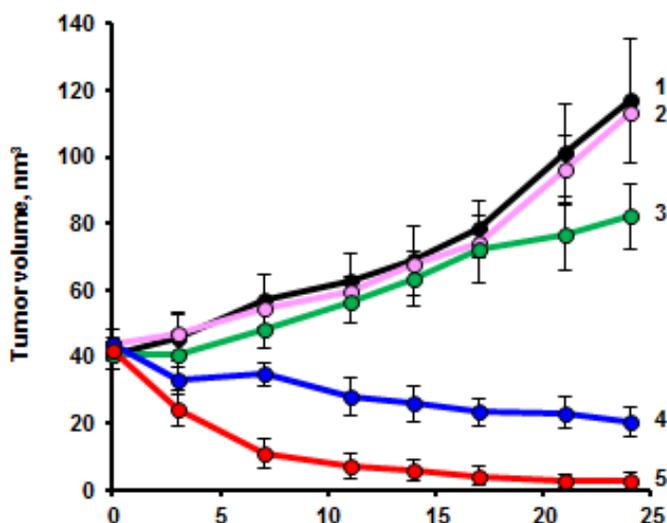
15

Figure 9. Changes in lung tumor volume after beginning of treatment. Mice were treated on days 0, 3, 7, 11, 14, 17, 21, and 24. 1 – Untreated mice; 2 – LHRH-NLC (inhalation); 3 – TAX (i.v.); 4 – LHRH-NLC-TAX (inhalation); 5 – LHRH-NLC-TAX-siRNAs targeted to MRP1 and BCL2 mRNAs (inhalation). Means ± SD are shown.

Treatment with free unbound TAX partially slowed down the growth of the tumor (curve 3 in Fig. 9). In this case the tumor volume at the end of the experiment was 82.2 ± 9.8 mm^3 ($P < 0.05$ when compared with untreated control). The conjugation of TAX to the NLC targeted to tumor cells by LHRH and local delivery by inhalation significantly enhanced antitumor activity of TAX (curve 4 in Fig. 9). After treatment with LHRH-NLC-TAX the tumor size decreased at the end of the experiment down to 20.8 ± 4.4 mm^3 ($P < 0.05$ when compare both with initial tumor volume at day 0 and untreated animals at day 24). Finally, the suppression of both pump and nonpump cellular drug resistance in lung cancer cells led to almost complete regression of the tumor (curve 5 in Fig. 9). In fact, the tumor size in animals treated with LHRH-NLC-TAX-siRNAs (MRP1 and BCL2) shrank down to 2.6 ± 3.0 mm^3 ($P < 0.05$ when compared with other treatments and initial tumor volume). It should also be stressed that in 50% of animals the level of bioluminescence of cancer cells in the lungs was below the detectable limit of the optical systems used. These findings indicate almost complete disappearance of lung tumor in experimental animals. In these cases other imaging techniques also were not able to detect lung tumor after the treatment with LHRH-NLC-TAX-siRNAs.

Discussion

The ultimate goal of the present study was the development of a multifunctional tumor targeted system capable of delivering an anticancer drug simultaneously with siRNA specifically to the lung tumor. We used nanostructured lipid carriers as a vehicle to achieve this goal. In this system, NLC was used as carriers, an anticancer drug served as cell death inducer and siRNA as a suppressor of cellular drug resistance in cancer cells. Previously, we identified MRP1 and BCL2 mRNA as major targets to suppress pump and nonpump cellular resistance in lung cancer cells, respectively [11, 17, 22, 34]. Consequently, in order to simultaneously suppress both types of cellular resistance in lung cancer cells, two types of siRNA molecules were used. The first type of siRNA was targeted to MRP1 mRNA and was used to suppress the main drug efflux transporter in lung cancer cells. The second type was targeted to BCL2 mRNA and was used to suppress cellular antiapoptotic defense – the main component of nonpump resistance. In order to deliver active components of the NLCS specifically to the lungs, local delivery by inhalation of NLCS was used. The inhalation delivery led to the preferential accumulation of NLCS in the lungs when

compared with accumulation in other organs. In contrast, intravenous injection of the same nanosystem led to the predominant accumulation of NLCS in the liver, kidney and spleen, while much less amount of nanoparticles was found in the lungs. Such passive targeting by the local delivery to the lung substantially limited possible adverse side effects on healthy organs. To further target NLCS specifically to lung cancer cells, we utilized a synthetic analog of LHRH peptide as a targeting moiety in NLCS. Previously, we found that LHRH receptors are overexpressed in different cancer cells (including lung cancer cells) and are not expressed to a detectable level in healthy visceral organs [18-20, 27, 28, 32, 39, 41, 42]. Therefore, the present experimental treatment approach involves a dual targeting of NLCS. On the one hand, inhalation provides for a local delivery of therapeutics directly to the lungs (passive targeting). On the other hand, targeting of the NLCS specifically to lung cancer cells by LHRH (active targeting) enforces a preferential accumulation of active components in lung cancer cells leaving healthy lung cells intact. Data obtained in the present investigation support the proposed dual targeting approach. We found that LHRH-targeted NLCS after inhalation accumulated predominately in the lungs and more specifically in the lung cancer cells. Hence, the use of LHRH as a cancer-targeting moiety adds specificity to the NLCS and enhances tumor targeted drug delivery by combining a passive lung targeting (local inhalation delivery) with powerful active targeting specifically to cancer cells (LHRH peptide).

To effectively perform their action, all active components should be delivered into the cancer cell, distributed inside the cell in right compartments and preserve their specific activity. Data obtained in the present study clearly show that the proposed NLC-based tumor targeted delivery system penetrates cancer cells and delivers its payload. Different anticancer drugs can have different mechanisms of action and require cytoplasmic or nuclear delivery in order to induce cell death. For example, the major mechanism of DOX involves DNA damage through topoisomerase II inhibition and DNA intercalation [43, 44]. Consequently, it should be delivered into the nucleus in order to effectively kill cancer cells. In contrast, siRNA acts in the cytoplasm via the RNA interference [45]. Therefore, the primary localization of delivered siRNA inside the cells should be in the cytoplasm. We found that the proposed targeted NLCS is capable of transporting an anticancer drug both in the cytoplasm and cellular nuclei, while delivered siRNA was predominately localized in the cytoplasm. We found that TAX delivered by targeted NLCS inside cancer cells efficiently induced cell death in lung cancer cells and slowed down the progression of lung tumor or even completely eliminated it. Similarly, both types of siRNA (targeted to MRP1 and BCL2 mRNAs) after the release from the NLCS were capable to silence targeted genes. Consequently, the proposed NLCS provided for an effective intracellular delivery of anticancer drugs and siRNA in the required compartments of cancer cells and delivered components were capable to perform their major functions – induction of cell death and silencing of targeted genes specifically in lung tumor cells.

Our previous investigations showed that for effective killing of cancer cells, cell death induction should be accompanied with the suppression of cellular drug resistance and identified the major mechanisms of such resistance. We termed two main components of drug resistance as "pump" and "nonpump" resistance [10, 11, 17]. So-called pump resistance is mainly caused by the active efflux of anticancer drugs by drug efflux pumps. The second major component of cellular drug resistance includes mechanisms that prevent the progression of cellular damage caused by an anticancer drug into cell death, but do not

involve drug efflux pumps. It may include drug detoxification mechanisms, interruption or inhibition of cell death signal, mechanisms of repairing of cellular damage on different levels, antioxidant defense, *etc*. However, the most powerful mechanism of nonpump cellular resistance in many cancer cells is antiapoptotic defense. Our previous investigations identified MRP1 and BCL2 proteins as major players in pump and nonpump resistance, respectively, in lung cancer cells [11, 17, 28, 34]. Consequently, two types of siRNA targeted to MRP1 and BCL2 mRNA were included into the proposed NLCS for local inhalation delivery to the lungs. Data obtained showed that suppression of both pump and nonpump resistance substantially enhanced anticancer activity of the chemotherapeutic drug and led to the effective cell death induction, killing of cancer cells and regression in the growth of lung tumors or almost complete tumor disappearance. Therefore, the proposed NLCS effectively performed its multifunctional task providing simultaneous cell death induction and suppression of drug resistance in lung cancer cells.

Conclusions

The proposed nanocarrier-based targeted delivery system demonstrated high efficiency in delivering of anticancer drugs and two types of siRNA specifically to lung tumor cells via inhalation. It accumulated predominately in the lungs and more specifically in lung cancer cells leaving healthy organs and non-tumorous lung cells intact. The system also showed enhanced antitumor efficiency when compared with free drug or similar system delivered intravenously.

Acknowledgements

Figure legends

Figure 1. A schematic representation of Nanostructured Lipid Carrier (NLC)-based drug delivery system for pulmonary co-delivery of an anticancer drug, siRNA and targeting peptide.

Figure 2. Characterization of LHRH-targeted paclitaxel (TAX)-loaded Nanostructured Lipid Carriers (LHRH-NLC-TAX-siRNA). (A) Size distribution of LHRH-NLC-TAX-siRNA measured by dynamic light scattering before and after nebulization. (B) Atomic Force Microscope image of LHRH-NLC-TAX-siRNA.

Figure 3. Complexation of siRNA with NLC. (A) A representative agarose gel electrophoresis image illustrating siRNA complexation efficiency by LHRH-NLC-TAX at the following w/w ratio (weight NLC/weight siRNA): (1) 0:1 (naked siRNA, control); (2) 10:1; (3) 50:1; (4) 100:1; and (5) 117:1. Complexation of siRNA prevented staining of siRNA by

ethidium bromide and led to the disappearance of the siRNA band. Therefore, the fluorescent intensity of the siRNA band on the gel (well 5) disappeared when siRNA was complexed with NLC at w/w ratio = 117:1. (B) siRNA complexation efficiency of LHRH-NLC-TAX evaluated by the ethidium bromide dye displacement assay. The arrow on the curve highlights the w/w ratio corresponding to the apparent end of siRNA complexation with NLC. Means ± SD are shown.

Figure 4. Viability of multidrug-resistant H69AR human lung cancer cells incubated for 48 hours with the indicated formulations. A, cytotoxicity of formulations that do not contain DTAX; B, cytotoxicity of formulations that contain TAX. Means ± SD are shown. *$P < 0.05$ when compared with control.

Figure 5. Accumulation of NLC in the lung tissues after the inhalation delivery (A) and intracellular localization of the drug and siRNA released from NLC (B-E). Representative transmission electron microscopy image of NLC labeled with osmium tetroxide in lung tissues (A). Representative images of A549 human lung cancer cells incubated 3 h with LHRH-NLC-DOX-siRNA: (B) visible light; (C) fluorescence images of nuclei stained with DAPI; (D) and (E) cellular localization of DOX (red fluorescence) and fluorescently labeled siRNA (green fluorescence), respectively.

Figure 6. Expression of *MRP1* (A), *BCL2* (B) and β_2-m (C and D, internal standard) genes. Representative images of RT-PCR products and densitometric analysis of bands in A549 lung cancer cells incubated with the following formulations: (1) Control (medium); (2) LHRH-NLC-TAX; and (3) LHRH-NLC-TAX-siRNAs (MRP1 and BCL2). Gene expression in control was set to 100%. Means ± SD are shown. *$P < 0.05$ when compared with control.

Fig.7. Evaluation of orthotopic lung cancer model by imaging. (A) Bioluminescence optical imaging of control mouse and mice with lung tumors of different size. (B-D) Magnetic resonance imaging of control mouse (B) and mice with lung tumors of different size (C, D). Lung tumor (blue) and healthy lung tissues (red) are shown (D). (E) Optical imaging of excised organs. (F-G) Computed tomography images of control mouse (F) and mouse with lung tumors (G). (H) Visualization of lung tumor by ultrasound imaging system.

Figure 8. Accumulation of NLC in the lungs and other organs. (A) Organ distribution of fluorescently labeled (Cy5.5) NLC in mice after i.v. (left) and inhalation (right) administration. (B) Distribution of fluorescently labeled (Cy5.5) non-targeted and LHRH-tumor targeted NLC in mouse lungs bearing human lung cancer. (C) Distribution of fluorescently labeled (Cy5.5) LHRH-tumor - targeted (NLC-LHRH) in mouse lungs bearing human lung tumor cells (tumor and non-tumor tissues; bright field and fluorescence microscope images; red color represents distribution of NLC-LHRH in tumor and non-tumor lung tissues).

Fig. 9. Changes in lung tumor volume after beginning of treatment. Mice were treated on days 0, 3, 7, 11, 14, 17, 21, and 24. 1 – Untreated mice; 2 – LHRH-NLC (inhalation); 3 – TAX (i.v.); 4 – LHRH-NLC-TAX (inhalation); 5 – LHRH-NLC-TAX-siRNAs targeted to MRP1 and BCL2 mRNAs (inhalation). Means ± SD are shown.

References

[1] Carbone DP, Felip E. Adjuvant therapy in non-small cell lung cancer: future treatment prospects and paradigms. Clinical lung cancer 2011; 12: 261-71.

[2] Francis H, Solomon B. The current status of targeted therapy for non-small cell lung cancer. Internal medicine journal 2010; 40: 611-8.

[3] Higgins MJ, Ettinger DS. Chemotherapy for lung cancer: the state of the art in 2009. Expert review of anticancer therapy 2009; 9: 1365-78.

[4] Katzel JA, Fanucchi MP, Li Z. Recent advances of novel targeted therapy in non-small cell lung cancer. Journal of hematology & oncology 2009; 2: 2.

[5] Wagner TD, Yang GY. The role of chemotherapy and radiation in the treatment of locally advanced non-small cell lung cancer (NSCLC). Current drug targets 2010; 11: 67-73.

[6] Carvalho TC, Carvalho SR, McConville JT. Formulations for pulmonary administration of anticancer agents to treat lung malignancies. Journal of aerosol medicine and pulmonary drug delivery 2011; 24: 61-80.

[7] Densmore CL. The re-emergence of aerosol gene delivery: a viable approach to lung cancer therapy. Current cancer drug targets 2003; 3: 275-86.

[8] Gautam A, Koshkina N. Paclitaxel (taxol) and taxoid derivates for lung cancer treatment: potential for aerosol delivery. Current cancer drug targets 2003; 3: 287-96.

[9] Koshkina NV, Waldrep JC, Knight V. Camptothecins and lung cancer: improved delivery systems by aerosol. Current cancer drug targets 2003; 3: 251-64.

[10] Pakunlu RI, Cook TJ, Minko T. Simultaneous modulation of multidrug resistance and antiapoptotic cellular defense by MDR1 and BCL-2 targeted antisense oligonucleotides enhances the anticancer efficacy of doxorubicin. Pharmaceutical research 2003; 20: 351-9.

[11] Pakunlu RI, Wang Y, Tsao W, Pozharov V, Cook TJ, Minko T. Enhancement of the efficacy of chemotherapy for lung cancer by simultaneous suppression of multidrug resistance and antiapoptotic cellular defense: novel multicomponent delivery system. Cancer research 2004; 64: 6214-24.

[12] Amaral L, Engi H, Viveiros M, Molnar J. Review. Comparison of multidrug resistant efflux pumps of cancer and bacterial cells with respect to the same inhibitory agents. In vivo 2007; 21: 237-44.

[13] Merino V, Jimenez-Torres NV, Merino-Sanjuan M. Relevance of multidrug resistance proteins on the clinical efficacy of cancer therapy. Current drug delivery 2004; 1: 203-12.

[14] O'Connor R. The pharmacology of cancer resistance. Anticancer research 2007; 27: 1267-72.

[15] Ozben T. Mechanisms and strategies to overcome multiple drug resistance in cancer. FEBS letters 2006; 580: 2903-9.

[16] Pakunlu RI, Wang Y, Saad M, Khandare JJ, Starovoytov V, Minko T. In vitro and in vivo intracellular liposomal delivery of antisense oligonucleotides and anticancer drug. Journal of controlled release : official journal of the Controlled Release Society 2006; 114: 153-62.

[17] Saad M, Garbuzenko OB, Minko T. Co-delivery of siRNA and an anticancer drug for treatment of multidrug-resistant cancer. Nanomedicine 2008; 3: 761-76.

[18] Chandna P, Khandare JJ, Ber E, Rodriguez-Rodriguez L, Minko T. Multifunctional tumor-targeted polymer-peptide-drug delivery system for treatment of primary and metastatic cancers. Pharmaceutical research 2010; 27: 2296-306.

[19] Dharap SS, Wang Y, Chandna P, Khandare JJ, Qiu B, Gunaseelan S, Sinko PJ, Stein S, Farmanfarmaian A, Minko T. Tumor-specific targeting of an anticancer drug delivery system by LHRH peptide. Proc Natl Acad Sci U S A 2005; 102: 12962-7.

[20] Taratula O, Garbuzenko OB, Kirkpatrick P, Pandya I, Savla R, Pozharov VP, He H, Minko T. Surface-engineered targeted PPI dendrimer for efficient intracellular and intratumoral siRNA delivery. Journal of controlled release : official journal of the Controlled Release Society 2009; 140: 284-93.

[21] Taratula O, Garbuzenko O, Savla R, Wang YA, He H, Minko T. Multifunctional nanomedicine platform for cancer specific delivery of siRNA by superparamagnetic iron oxide nanoparticles-dendrimer complexes. Current drug delivery 2011; 8: 59-69.

[22] Taratula O, Garbuzenko OB, Chen AM, Minko T. Innovative strategy for treatment of lung cancer: targeted nanotechnology-based inhalation co-delivery of anticancer drugs and siRNA. Journal of drug targeting 2011; 19: 900-14.

[23] Garbuzenko OB, Saad M, Betigeri S, Zhang M, Vetcher AA, Soldatenkov VA, Reimer DC, Pozharov VP, Minko T. Intratracheal versus intravenous liposomal delivery of siRNA, antisense oligonucleotides and anticancer drug. Pharmaceutical research 2009; 26: 382-94.

[24] Kuruba R, Wilson A, Gao X, Li S. Targeted delivery of nucleic-acid-based therapeutics to the pulmonary circulation. The AAPS journal 2009; 11: 23-30.

[25] Uner M. Preparation, characterization and physico-chemical properties of solid lipid nanoparticles (SLN) and nanostructured lipid carriers (NLC): their benefits as colloidal drug carrier systems. Pharmazie 2006; 61: 375-86.

[26] Conn PM, Hazum E. Luteinizing hormone release and gonadotropin-releasing hormone (GnRH) receptor internalization: independent actions of GnRH. Endocrinology 1981; 109: 2040-5.

[27] Saad M, Garbuzenko OB, Ber E, Chandna P, Khandare JJ, Pozharov VP, Minko T. Receptor targeted polymers, dendrimers, liposomes: which nanocarrier is the most efficient for tumor-specific treatment and imaging? Journal of controlled release : official journal of the Controlled Release Society 2008; 130: 107-14.

[28] Zhang M, Garbuzenko OB, Reuhl KR, Rodriguez-Rodriguez L, Minko T. Two-in-one: combined targeted chemo and gene therapy for tumor suppression and prevention of metastases. Nanomedicine 2012; 7: 185-97.

[29] Huang ZR, Hua SC, Yang YL, Fang JY. Development and evaluation of lipid nanoparticles for camptothecin delivery: a comparison of solid lipid nanoparticles, nanostructured lipid carriers, and lipid emulsion. Acta pharmacologica Sinica 2008; 29: 1094-102.

[30] Li X, Nie SF, Kong J, Li N, Ju CY, Pan WS. A controlled-release ocular delivery system for ibuprofen based on nanostructured lipid carriers. International journal of pharmaceutics 2008; 363: 177-82.

[31] Zhang XG, Miao J, Dai YQ, Du YZ, Yuan H, Hu FQ. Reversal activity of nanostructured lipid carriers loading cytotoxic drug in multi-drug resistant cancer cells. International journal of pharmaceutics 2008; 361: 239-44.

[32] Chandna P, Saad M, Wang Y, Ber E, Khandare J, Vetcher AA, Soldatenkov VA, Minko T. Targeted proapoptotic anticancer drug delivery system. Molecular pharmaceutics 2007; 4: 668-78.

[33] Patil ML, Zhang M, Betigeri S, Taratula O, He H, Minko T. Surface-modified and internally cationic polyamidoamine dendrimers for efficient siRNA delivery. Bioconjugate chemistry 2008; 19: 1396-403.

[34] Garbuzenko OB, Saad M, Pozharov VP, Reuhl KR, Mainelis G, Minko T. Inhibition of

lung tumor growth by complex pulmonary delivery of drugs with oligonucleotides as suppressors of cellular resistance. Proceedings of the National Academy of Sciences of the United States of America 2010; 107: 10737-42.

[35] Mainelis G, Seshadri S, Garbuzenko OB, Han T., Wang Z, Minko T. Characterization and application of a nose-only exposure chamber for inhalation delivery of liposomal anti-cancer drugs and nucleic acids to mice. J. Aerosol Med. 2013; in press:

[36] Minko T, Kopeckova P, Kopecek J. Efficacy of the chemotherapeutic action of HPMA copolymer-bound doxorubicin in a solid tumor model of ovarian carcinoma. International journal of cancer. Journal international du cancer 2000; 86: 108-17.

[37] Betigeri S, Zhang M, Garbuzenko O, Minko T. Non-viral systemic delivery of siRNA or antisense oligonucleotides targeted to Jun N-terminal kinase 1 prevents cellular hypoxic damage. Drug Deliv Transl Res 2011; 1: 13-24.

[38] Wang Y, Saad M, Pakunlu RI, Khandare JJ, Garbuzenko OB, Vetcher AA, Soldatenkov VA, Pozharov VP, Minko T. Nonviral nanoscale-based delivery of antisense oligonucleotides targeted to hypoxia-inducible factor 1 alpha enhances the efficacy of chemotherapy in drug-resistant tumor. Clin Cancer Res 2008; 14: 3607-16.

[39] Khandare JJ, Chandna P, Wang Y, Pozharov VP, Minko T. Novel polymeric prodrug with multivalent components for cancer therapy. The Journal of pharmacology and experimental therapeutics 2006; 317: 929-37.

[40] Mainelis G, Seshadri S, Garbuzenko OB, Han T, Wang Z, Minko T. Characterization and Application of a Nose-Only Exposure Chamber for Inhalation Delivery of Liposomal Drugs and Nucleic Acids to Mice. Journal of aerosol medicine and pulmonary drug delivery 2013 Mar 26. [Epub ahead of print];

[41] Dharap SS, Qiu B, Williams GC, Sinko P, Stein S, Minko T. Molecular targeting of drug delivery systems to ovarian cancer by BH3 and LHRH peptides. Journal of controlled release : official journal of the Controlled Release Society 2003; 91: 61-73.

[42] Dharap SS, Minko T. Targeted proapoptotic LHRH-BH3 peptide. Pharmaceutical research 2003; 20: 889-96.

[43] Fornari FA, Randolph JK, Yalowich JC, Ritke MK, Gewirtz DA. Interference by doxorubicin with DNA unwinding in MCF-7 breast tumor cells. Molecular pharmacology 1994; 45: 649-56.

[44] Momparler RL, Karon M, Siegel SE, Avila F. Effect of adriamycin on DNA, RNA, and protein synthesis in cell-free systems and intact cells. Cancer research 1976; 36: 2891-5.

[45] Bagasra O, Prilliman KR. RNA interference: the molecular immune system. Journal of molecular histology 2004; 35: 545-53.